

Postural Models to Control Cable-Driven Parallel Robots For Rehabilitation: A Pilot Study on Squat Assistance

Robert M. Carrera¹, Yupei Cai¹, Keshu Cai¹, Xiangzhi Zhao¹, Vanshika Sriram¹, Sunil K. Agrawal¹

Abstract—A cable-driven parallel robot (CDPR) targeting multiple body segments can control assistive torques at different joints to assist in stable postural control. Assistive exoskeletons commonly use postural models to predict and supplement subject-generated joint torques. Rehabilitative CDPRs, however, have not previously used whole-body postural models to coordinate assistive torques across joints. We coordinated a CDPR’s shank and pelvic forces with a conceptual postural model and virtual reality (VR) motion trackers to provide targeted knee extension torque during a shallow squat. Twelve unimpaired subjects squatted under eight different assistance conditions. Visual feedback guided subjects to squat with consistent knee flexion, but each subject used unique kinematics and thus required differing amounts of knee torque assistance. A pelvic force with a large moment arm about the ankle failed to reduce knee extensor activation, altered ankle muscle activation, and affected center of pressure (COP) positioning relative to baseline. Conditions with a coordinated shank force added to this pelvic force or with a smaller pelvic force leverage about the ankle reduced knee extensor activation without disturbing ankle muscle activation or COP positioning. The results confirm that coordinating multisegment forces is critical for stable postural training and that a conceptual postural model driven by an affordable sensor system can accomplish this coordination. We discuss how coordinating multisegment CDPR forces could enable weight bearing and stable postural training in more severely impaired populations.

I. INTRODUCTION

Biomechanical models have been widely used both offline and in-the-loop to coordinate the control of exoskeletons [1]. Biomechanical models allow for the selection of appropriate joint torques that assist the subject’s movement. For example, model-based clinical gait analysis (CGA) is commonly used offline to estimate subject-generated joint torques throughout the gait cycle such that the exoskeleton can provide supplementary torques. Examples of in-the-loop model-based control include gravity compensation of the user’s mass in squatting and gait and controllers using reflex-based neuromuscular models (RNM)s or EMG-based control to predict muscle activation and resultant joint torques [2] [3], [1], [4], [5], [6]. Gravity compensation approaches have used conceptual models of posture that capture key features of the modeled segment’s movements [2], [3]. Examples of conceptual models include the single and double inverted pendulum models of stance and the 2- or 3-DOF kinematic model of the leg

This work was partially supported by the Spinal Cord Injury Board of the New York State Department of Health under award number C3XXX.

¹Mechanical Engineering, Columbia University, New York, NY USA.

† Corresponding author: sa3077@columbia.edu

in the sagittal plane [7], [8]. RNM exoskeleton controllers and EMG-based controllers typically employ kinematically simple conceptual models with additional elements modeling neuromuscular control [1], [4], [5].

Cable-driven parallel robots (CDPRs) present different control challenges than do exoskeletons. In stance or gait applications, CDPRs targeting only a single body segment generate torques at all joints involved in transmitting forces between the targeted body segment and the ground. For example, cables routed from a frame surrounding the subject to the pelvis will generate torques about the hip, knee, and ankle joints. These torques can be desirable in that they increase or decrease activation of a targeted muscle group or lead to a desired movement of the pelvis. The TPAD CDPR applied a downward force to the pelvis of children with crouch gait while walking on a treadmill, increasing soleus activation and eliciting postural and kinematic improvements [9]. A gait training robot for toddlers used a CDPR to control pelvis position along a desired trajectory [10]. However, CDPR-generated joint torques can also be undesirable when, in an unintended way, proper performance of the task requires the user to compensate for generated joint torques. For example, a posteriorly-directed pelvic force applied to a person leaning forward with the knees extended might achieve a goal of counteracting dorsiflexing ankle torques, but it would also generate substantial knee flexion torques that the person would have to counteract to keep the knee extended. In application, CDPRs have often used position control of a targeted segment and accepted that the user may have to compensate for undesirable joint torques. Likewise, some simulated CDPRs that apply forces to the swing leg neglect torques generated on the stance leg’s joints [11], [8], [12]. Possibly, this is because CDPRs have often applied relatively small assistive, perturbative, or resistive forces in those with mild to moderate impairments, for example, those who can already walk on a treadmill.

Biomechanical models have previously been incorporated in CDPR controllers, but not to control joint torques in a postural application. As mentioned, several simulated CDPRs have proposed applying forces to multiple segments of the kinematically modeled swing leg to control joint torques [8], [12]. The STRINGMAN robot applied forces to the torso and pelvis via cables and used a complex biomechanical model to estimate ground reaction forces for zero moment point (ZMP) control, but did not consider generated joint torques [13].

The Robotic Upright Stand Trainer (RobUST) applies forces to the body via chest, pelvis, or shank cables. Previously, the system has only applied forces to the pelvis and/or chest

to influence their position independently, without considering generated joint torques or the need for intersegment coordination [14], [15]. This work incorporates a conceptual postural model of the user into the RobUST's control loop, enabling torque control at key model joints. This coordination prevents one segment force from creating posturally destabilizing joint torques by letting another segment force provide counteracting torques. To our knowledge, this paper presents the first use of a whole-body postural model for CDPR control via control of the model's joint torques.

We validate the approach by assisting unimpaired subjects in performing a shallow squat, showing that coordinated pelvis-shank gravity compensation assistance can reduce knee flexor muscle activity without altering EMG activity at the ankle joint. As vertical forces create very little knee torque near the upright posture, we explore pelvis-shank assistance with both a vertical pelvic force and a pelvic force normal to the model's thigh segment. We contrast coordinated pelvis-shank assistance, pelvis-only assistance, and squatting with handlebars, which people with impairments commonly use for practicing sit-to-stand [16]. We also examine how different types of assistance affected the vertical ground reaction force (GRF), center of pressure (COP), and pelvic and chest trajectories.

II. METHODS

A. Experimental Procedure

Twelve unimpaired adults (median age = 24, 7 men and 5 women) participated in the experiment. Each subject gave consent to participate under protocol AAAR6780, which was approved by the Columbia University Institutional Review Board.

Subjects wore wireless Delsys Trigno surface EMG sensors on the soleus (SOL), tibialis anterior (TA), vastus medialis (VM), biceps femoris (BF), and gluteus medius (GluMd) bilaterally. Each subject also wore a chest belt at roughly the mid-sternum, a climbing harness which sat above the iliac crest and which had additional straps worn around each thigh, and bilateral shank belts which were positioned just below the knee. Vive trackers on each belt and an additional tracker on the robot frame tracked subject movements in the model's base frame, frame 0.

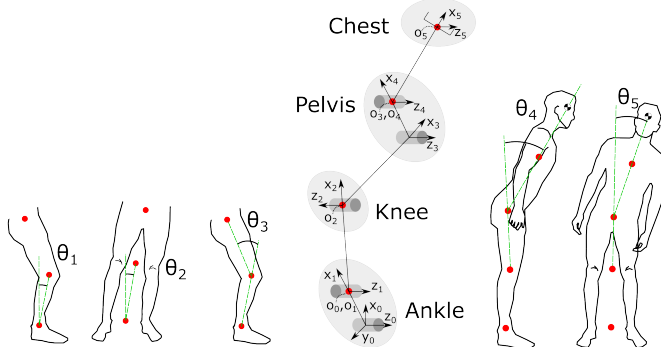


Fig. 1. A 5-DOF, 3-link model of stance. Links represent the shank, thigh, and upper body. Links are shown as green dotted lines connecting red circles on the subject silhouettes and as black lines linking shaded regions in the kinematic model diagram.

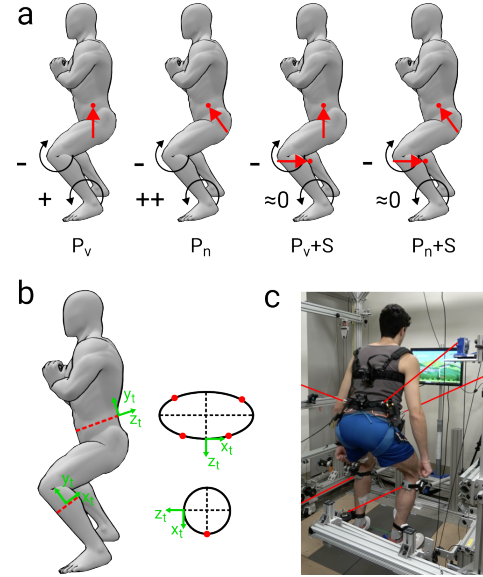


Fig. 2. **a)**: The four types of robotic squatting assistance. Assistive forces and corresponding expected joint torques are shown as red and black arrows, respectively. From left to right: pelvic vertical force (P_v), pelvic force normal to knee-pelvis line (P_n), pelvic vertical force and shank force (P_v+S), pelvic normal force and shank force (P_n+S). The pelvic normal condition maximizes the moment arm of the pelvic force about the knee. The shank force acts to counteract pelvis-generated, dorsiflexing ankle torque in the sagittal plane. **b.)** The subject wears belts on the pelvis and on the shanks bilaterally which transmit cable forces to the wearer. Offsets from the Vive tracker (green) coordinate frames determine the body segment centers (intersection of dashed lines) and cable attachment points (red dots). **c.)** A subject performing the squatting task. Visible cables are highlighted in red.

Subjects squatted with each foot on a Bertec portable force plate while connected to the four pelvic cables and two shank cables. A screen provided visual feedback of the knee angle to the user. The screen presented a two-link kinematic model representing the shank and thigh of the user. A pink model showed the subject's current knee angle, and a white model showed the target knee angle at the bottom of the squat. Notably, the onscreen link representing the shank was fixed in a vertical orientation and did not move. As a result, only knee angle information was presented to the subject and there was not an explicit target shank (θ_1) or trunk (θ_4) angle. However, instructions were provided to encourage a typical squat posture. Before the experiment began, a researcher explained and demonstrated an ideal squat in which the shanks were kept relatively vertical and the trunk was kept upright.

Subjects completed six squats in nine different squatting conditions. Even-numbered subjects completed the conditions in the forward order (T_i , HB, $P_{v,24}$, $P_{n,24}$, $P_{v,24} + S$, $P_{v,36} + S$, $P_{n,24} + S$, $P_{n,36} + S$, T_f). The first (T_i) and last (T_f) conditions were completed with the robot in “transparent mode,” in which the robot minimized interference with the squat by maintaining a baseline cable tension of 15 N in each cable. Before the T_i condition, subjects were instructed to find and maintain a comfortable stance at shoulder width or slightly wider. The positions of the feet were marked with tape immediately after the T_i condition to ensure consistent foot placement. In the handlebar condition (HB), subjects

maintained a grip on parallel handlebars oriented parallel to the sagittal plane and positioned at a height such that the elbows were slightly flexed with the hands located at the sides of the pelvis. For the HB condition, subjects were told to “use the handlebars as you would like to make squatting easier for you.” Two conditions included only a pelvic force to assist in knee extension: a vertical pelvic force ($P_{v,24}$) and a pelvic force normal to the model’s thigh link ($P_{n,24}$), each compensating for 24% of the gravity torque at the knee. Importantly, the vertical pelvic forces were only applied at 50° of knee flexion or more, as vertical forces had little leverage about the knee near the upright position and a very large force would be required to generate the desired knee torque. Four conditions included a pelvic force for knee extension and a shank force to balance torque at the ankle in the sagittal plane (i.e., about θ_1). These included a vertical ($P_{v,24} + S$, $P_{v,36} + S$) or normal ($P_{n,24} + S$, $P_{n,36} + S$) pelvic force which compensated for either 24% or 36% of the gravity torque about the knee. Fig. 2 shows the four types of robotic assistance.

B. The Postural Model

The biomechanical model is presented in Fig. 1. The model was a serial kinematic chain with only a single leg. The model has a 2-DOF universal joint at the ankle, a revolute joint at the knee, and a 2-DOF universal joint located at the pelvic center. In a typical shoulder-width squat posture, the angles [θ_1 , θ_2 , θ_3 , θ_4] roughly correspond with ankle plantar/dorsiflexion, ankle inversion/eversion, knee flexion, combined hip flexion/extension and lumbothoracic flexion/extension, respectively. θ_5 can be influenced by various joint angles including pelvic rotation, hip flexion, pelvic obliquity, and lateral bending, but should be relatively small. The model’s base frame, frame 0, is established relative to the Unity software’s global reference frame using the reference tracker and the two ankle trackers, with its origin at the mid-ankle position. Segment masses were assigned using anthropometric parameters for the shank, thigh, and one-segment torso (see supplemental materials for details) [17].

C. Inverse Kinematics with the VR trackers

The location of the four terminal pelvic pulleys and the two terminal shank pulleys were determined relative to the reference tracker using the Vicon Vero retroreflective optical tracking system.

To determine body segment centers and cable attachment points, the shank, pelvis, and chest cross-sectional perimeters were modeled as 2D profiles in the x-z plane of the segment’s tracker (Fig. 2). The shank cross-section was modeled as a circle, whereas the pelvis and chest cross-sections were modeled as ellipses. The mediolateral (ML) and anteroposterior (AP) dimensions of the pelvis and chest ellipses were measured manually. We computed the shank radius by measuring the shank perimeter. To determine the shank, pelvis, and chest centers, the circle radius or half of the ellipse AP axis plus an offset accounting for the width of the tracker mount were added to the tracker position along the tracker’s negative z-axis.

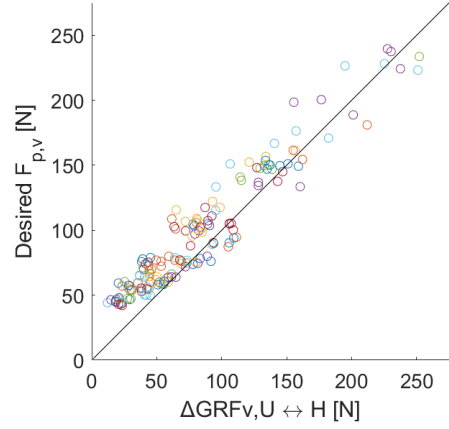


Fig. 3. Trial data in subject-specific colors shows that the desired vertical force component at the pelvis during the squat hold closely follows the change in vertical ground reaction force (GRF) from the upright position to the squat hold (root mean square error = 21.8 N).

We assumed that cable attachment points were located along the perimeter of the circular or elliptical segment models. The linear distances from the pelvic tracker to the pelvic belt attachments were measured manually for each pelvic belt size and used to compute locations on the ellipse. The shank cable attachment is displaced from the shank center by one radius along the tracker’s positive (left shank) or negative (right shank) x-axis (x_t).

After body segment centers and cable attachment points were computed in the local tracker frame and pulley centers were located in the reference tracker frame, they were transformed to the base frame, or frame 0, of the biomechanical model. The model joint angles were computed using inverse kinematics and the knee, pelvis, and chest segment centers. The model’s Denavit-Hartenberg (DH) parameters and the solution for the model’s inverse kinematics are presented in the supplemental materials.

D. Coordinating Assistive Forces with the Postural Model

A serial chain model has the joint-space dynamic equations

$$M(\vec{q})\ddot{\vec{q}} + C(\vec{q}, \dot{\vec{q}}) + G(\vec{q}) = \vec{\tau}_{int} + \vec{\tau}_{ext} \quad (1)$$

where $M(\vec{q}) \in R^{nxn}$ is the inertia matrix, $C(\vec{q}, \dot{\vec{q}}) \in R^{nx1}$ is the vector of Coriolis and centripetal torques, $G(\vec{q}) \in R^n$ is the vector of gravity torques, $\vec{\tau}_{ext} \in R^n$ is the vector of interaction torques generated by contact with the environment, and $\vec{\tau}_{int} \in R^n$ is the vector of passive and active subject-generated joint torques. In the quasistatic case, (1) simplifies to

$$G(\vec{q}) = \vec{\tau}_{int} + \vec{\tau}_{ext} \quad (2)$$

where for the RobUST $\vec{\tau}_{ext}$ are the control torques.

In the absence of external torques, the internal torques must balance the gravity torques to achieve equilibrium. External torques that reduce the gravity torques at a joint or multiple joints would lead to a reduction in required internal torque

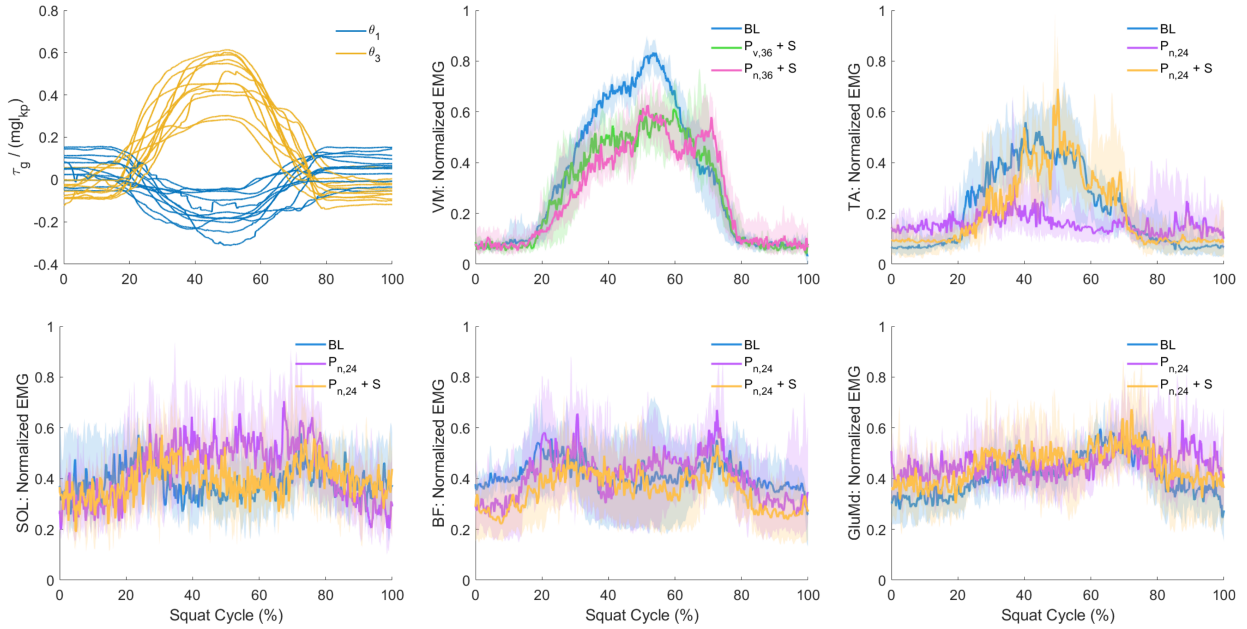


Fig. 4. **Top left:** The normalized mean gravity torques of the starting and ending transparent trials at the ankle joint, θ_1 , corresponding to ankle plantar/dorsiflexion, and at the knee joint, θ_3 , plotted against the squat cycle percentage. Gravity torques were normalized by the subject-specific estimated maximum gravity torque at the knee (see Section III-B). Each line represents a subject-specific mean. In the squat cycle, 0% and 100% correspond to the beginning of squat descent and the end of squat ascent, respectively. 50% corresponds to the middle of the squat hold. **Other plots:** The cohort's normalized median EMG for the vastus medialis (VM), tibialis anterior (TA), soleus (SOL), biceps femoris (BF), and gluteus medius (GluMd) throughout the squat cycle for selected assistance conditions. EMG was normalized by the per-subject maximum value of the mean EMG in a 500-ms sliding window in any transparent mode trial. Shaded regions extend to the third and first quartile.

generation. Here, we targeted a $(1 - c)$ fractional reduction in required internally generated knee torque,

$$\vec{\tau}_{ext} = [0 \ 0 \ cg_3 \ 0 \ 0]^T \quad (3)$$

$$\vec{\tau}_{int} = G(\vec{q}) - \vec{\tau}_{ext} = [g_1 \ g_2 \ (1 - c)g_3 \ g_4 \ g_5]^T \quad (4)$$

where c is a scalar between 0 and 1 and g_i indicates the gravity torque at joint i .

The cable-generated torques resulting from the applied shank and pelvis cable tensions can be computed as

$$\begin{aligned} \vec{\tau}_{ext} &= {}^0J_p^{T0}\vec{F}_p + {}^0J_s^{T0}\vec{F}_s \\ &= [J_{v,p}^T | J_{\omega,p}^T] \begin{bmatrix} \vec{F}_p \\ \vec{\tau}_p \end{bmatrix} \\ &\quad + [J_{v,s}^T | J_{\omega,s}^T] \begin{bmatrix} \vec{F}_s \\ \vec{\tau}_s \end{bmatrix} \end{aligned} \quad (5)$$

As the pelvis and shank cable vectors pass near to the center of their respective body segment, we assume the cable-generated segment torques $\vec{\tau}_s$ and $\vec{\tau}_p$ are zero. Note that the shank cables were directed approximately backwards (along $-\hat{y}_0$). For the desired vertical pelvic force, only the vertical (\hat{x}_0) component of the pelvic force is non-zero. For the desired normal pelvic force, ${}^0F_p \cdot \hat{n} = 0$, where \hat{n} is the unit vector from the knee center to the pelvic center. Simplifying notation, we denote the element in the i th row and j th column of ${}^0J_{v,p}^T$ and ${}^0J_{v,s}^T$ as $J_{p,ij}$ and $J_{s,ij}$, respectively. Let ${}^0F_{s,y}$ and ${}^0F_{p,x}$ denote the shank y-axis and pelvic x-axis force components in frame 0. We can then obtain the desired pelvic and shank forces that achieve partial gravity compensation by solving

$$\begin{bmatrix} \tau_1 = 0 \\ \tau_3 = cg_3 \end{bmatrix} = \begin{bmatrix} J_{s,12} & J_{p,11} \\ 0 & J_{p,31} \end{bmatrix} \begin{bmatrix} {}^0F_{s,y} \\ {}^0F_{p,x} \end{bmatrix} \quad (6)$$

$$\begin{bmatrix} \tau_1 = 0 \\ \tau_2 = 0 \\ \tau_3 = cg_3 \end{bmatrix} = \begin{bmatrix} J_{s,12} & J_{p,11} & J_{p,12} & J_{p,13} \\ 0 & n_x & n_y & n_z \\ 0 & J_{p,21} & J_{p,22} & J_{p,23} \\ 0 & J_{p,31} & J_{p,32} & J_{p,33} \end{bmatrix} \begin{bmatrix} F_{s,y} \\ {}^0F_p \\ F_{p,x} \end{bmatrix} \quad (7)$$

where (6) pertains to the vertical pelvic force and (7) pertains to the normal pelvic force.

E. Data Reduction and Statistical Analysis

EMG data was band-pass filtered with an 8th-order zero-phase Butterworth filter with cutoff frequencies $f_{low} = 20$ Hz and $f_{high} = 500$ Hz, rectified, and low-pass filtered with an 8th-order zero-phase Butterworth filter with cutoff frequency $f_{low} = 5$ Hz to obtain the EMG envelope. While many squatting studies analyze unilateral muscles, the mean iEMG signal of the bilateral muscles can be analyzed for symmetric tasks in which bilateral muscles are functionally coupled [18]. For simplicity, we averaged the integrated EMG (iEMG) signal of the bilateral muscles within time windows of interest.

A linear mixed model was used to conduct a repeated measures analysis to compare differences in mean values of the outcome variables by condition in R. The analysis is similar to a repeated measures ANOVA, but has several advantages including the retention of subjects who have incomplete data. The within-subjects factor was assistance condition. Dependent variables included integrated EMG during the squat hold

phase, changes in the vertical ground reaction force (GRF) and AP position of the COP from the upright posture to the squat hold, and the lock-step Euclidean distance (LSED, a measure of trajectory similarity; see supplemental material) between each condition's trajectories and the baseline condition trajectories [19]. If needed, dependent variables were log-transformed to achieve normality of residuals. We used post-hoc paired t-tests to determine significant differences between levels. When all conditions were compared to BL (7 comparisons), we applied Benjamini-Hochberg correction for multiple comparisons. For the four pre-planned comparisons between condition pairs ($P_{v,24}$; $P_{v,24} + S$), ($P_{n,24}$; $P_{n,24} + S$), ($P_{v,24} + S$; $P_{v,36} + S$), and ($P_{n,24} + S$; $P_{n,36} + S$), no correction was applied. There were only 4 extreme outliers across all dependent variables, and their removal did not affect the statistical significance of any comparisons. Key subject-specific mean values, cohort descriptive statistics by condition, and p-values are presented in plots. When baseline (BL) values or changes from BL are reported, the mean of the pre-test and post-test transparent conditions were taken as the BL value for each subject. Full statistics including the omnibus F-test p-value, degrees-of-freedom, and post-hoc t-test p-values are included as tables in the Supplemental Material.

A linear mixed model was also used to fit a linear regression to the change in VM activity from BL as a function of the subject-specific mean normalized knee gravity torque assistance in the squat hold. The model fitted subject-specific regression lines with a zero intercept, as no reduction in VM activity is expected when no assistance is provided.

Due to technical errors, the force plate data from three subjects was lost. Additionally, EMG data from two distinct subjects was lost for a single condition: condition $P_{v,24}$ for one subject and the initial transparent condition BL_{pre} for the other subject. In the latter case, the subject-specific BL represented the post-test transparent condition only.

III. RESULTS

A. Baseline Squat Kinematics and Assistive Force Application

The average knee flexion angle among all subjects in the squat hold was near 70° in all conditions: the smallest assistance condition median (interquartile range, IQR) was 69.42° (1.4°), the largest condition median was 70.5° (0.6°), and the largest condition knee angle IQR was 1.4° . In the BL condition, more between-subjects variability was observed for the ankle-knee plantarflexion (θ_1) angle and especially for the pelvis-chest angle in the sagittal plane (θ_4), with median (IQR) values for θ_1 of 29.4° (6.1°) and for θ_4 of 45.9° (27.4°). At the same time, the within-subject average standard deviation was relatively small for θ_1 (all-conditions median STD = 0.29° , subject max. STD = 2.5°) and θ_4 (all-conditions median STD = 0.8° , subject max. STD = 5.6°). θ_1 was relatively consistent from the pre- to the post-test transparent condition (post-minus pre-test: median = -0.7° , IQR = 2.6° , max. magnitude = 12.2°), whereas θ_4 showed more variability (post- minus pre-test: median = 6.2° , IQR = 17.2° , max. magnitude = -38.7°).

Fig. 3 compares the vertical component of the desired pelvic force with the change in vertical GRF from the upright

position to the squat hold position. The robot generated vertical forces close to the desired vertical force across the range of pelvic force magnitudes (root mean square (RMS) error = 21.8 N). The line of best fit had a slope of 0.831 , suggesting vertical GRF decreased in close proportion with increases in desired vertical pelvic force. However, a bias towards delivering vertical forces less than the desired vertical force was observed, particularly for smaller desired vertical forces.

Fig. 6 shows that, as expected, the decrease in vertical GRF from the upright position to the squat hold was largest in the pelvis vertical (P_v) conditions. Vertical GRF decreases were smaller in the pelvic normal (P_n) force conditions. Most subjects also bore little weight on the handlebars in the HB condition, as shown by small vertical GRF decreases.

B. Changes in Vastus Medialis EMG Activity

The VM acted to counteract flexion-inducing gravity torque at the knee during the squat descent, squat hold, and squat ascent phases (Fig. 4). The need to accelerate the body mass upwards out of the squat hold likely explains why peak VM activity occurred shortly after 50% of the squat cycle.

A plot of reduction in VM activity during the squat hold for the combined pelvis and shank force conditions shows that subjects received differing amounts of assistance depending on their posture in the squat hold (Fig. 5). The x-axis shows the desired knee torque, $\tau_{k,d} = c\tau_{g,3}$, which is proportional to the gravity torque at the knee, normalized by the product of the knee-to-pelvis length, l_{kp} , and the body weight above the shanks, $\tau_{kgmax} = (2m_{thigh} + m_{ub})gl_{kp}$. This normalization factor estimates the maximum possible knee torque, τ_{kgmax} , generated by the weight above the shanks acting at a distance l_{kp} , disregarding the fact that such a posture would likely be unstable. The thigh mass, m_{thigh} , and upper body mass, m_{ub} , were estimated from the total body mass and anthropometrics.

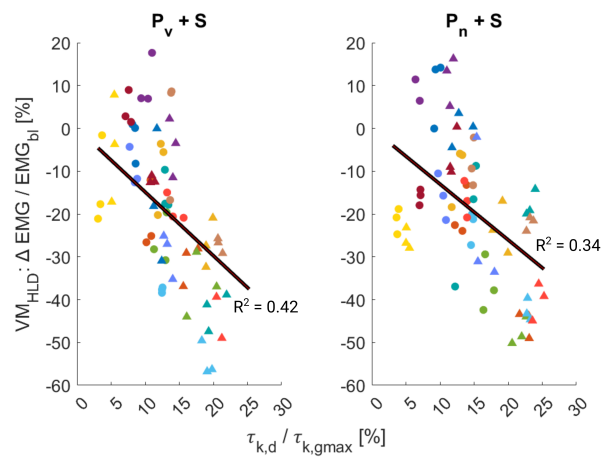


Fig. 5. Scatter plots of the desired knee torque assistance as a percent of the estimated, subject-specific maximum knee gravity torque plotted against the percent reduction in vastus medialis (VM) EMG activity from baseline. The final three trials from the 24% and 36% assistance conditions are shown as circles and triangles, respectively, in subject-specific colors. Group regressions from a linear mixed model with condition-specific slope as the fixed effects, random (i.e., per-subject) slopes, and a y-intercept of zero are shown in black (model adjusted $R^2 = 0.89$) with group regression R^2 values.

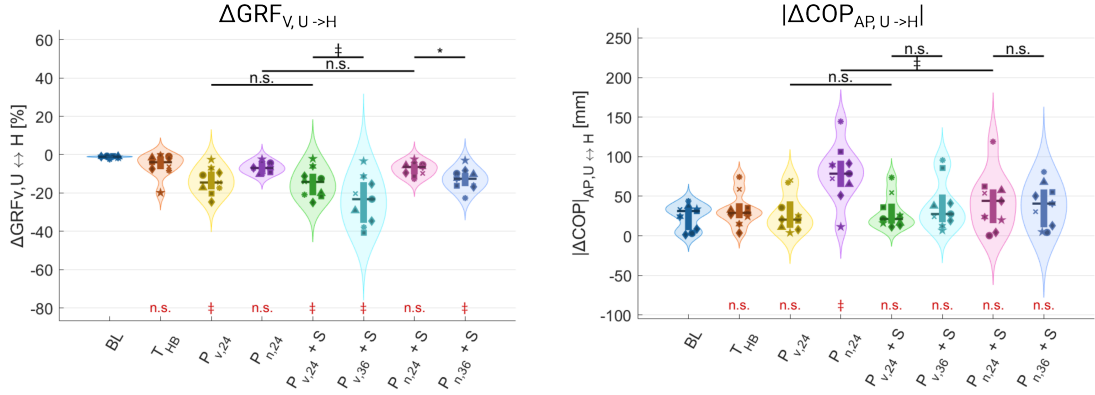


Fig. 6. Violin plots of the per-condition subject mean values for the kinematic and force plate variables. Statistical significance for comparisons between each condition and the baseline condition are shown below each violin (n.s. $\rightarrow p > 0.05$, * $\rightarrow p < 0.05$; † $\rightarrow p < 0.01$; ‡ $\rightarrow p < 0.001$). Select pairwise comparisons are shown with connecting bars and significance presented over the bar. Plots show the change in vertical ground reaction force (ΔGRF_v) and anteroposterior (AP) position of the center of pressure (ΔCOP_{AP}) from standing upright to the squat hold.

The LMM regression with zero intercept and subject-specific slopes fit the data well (adjusted $R^2 = 0.89$). The LMM group regression line ($P_v + S$ adjusted $R^2 = 0.42$, $P_n + S$ adjusted $R^2 = 0.34$) suggested that, despite the subject-specific variability in the degree of assistance provided, increasing knee torque assistance correlated with decreases in VM activity from baseline in both the pelvis vertical with shank assistance ($P_v + S$) and pelvis normal with shank assistance ($P_n + S$) conditions for most subjects. The slopes of the LMM regression lines for the $P_v + S$ and $P_n + S$ groups were not significantly different ($F(1,142) = 0.166$, $p = 0.685$).

The violin plot of VM iEMG activity in each condition relative to baseline (Fig. 7) shows that all robotic assistance conditions except the pelvic normal force without shank assistance ($P_{n,24}$) decreased VM activity relative to the transparent baseline conditions. Within the pelvic normal or vertical force with shank assistance conditions ($P_v + S$ and $P_n + S$), 36% assistance decreased VM activity more than 24% assistance. The handlebar condition (HB) failed to significantly decrease VM activity, as most subjects chose to bear little weight on the handlebars.

C. Changes in the Ankle Muscle EMG Activity

The TA was most active during the squat hold, while the SOL had periods of increased activity during squat descent and ascent and was relatively inactive during the squat hold (Fig. 4).

For both the SOL and TA, a variable response in the EMG activity during the squat hold was seen in most assistance conditions, with some subjects showing increased activity and others showing decreased activity (Fig. 7). As a result, the mean change from BL was not significant in any condition except for the pelvic normal force without shank force ($P_{n,24}$) condition ($p = 0.0010$). The ($P_{n,24}$) condition reduced TA activity during the squat hold for 10 of 12 subjects, with a median (interquartile range, IQR) iEMG change from baseline of -45.8% (53.3%). Adding a shank force to compensate for the ankle torques generated by the pelvic normal force ($P_{v,24} + S$ condition) prevented this reduction in TA activity

and led to a more typical range of TA activation changes that was not significantly different from BL ($p = 0.8553$) and significantly less than $P_{n,24}$ ($p = 0.0005$). The ($P_{n,24}$) condition also trended (non-significantly, $p = 0.1560$) towards increasing SOL activity during the squat hold from baseline by a median (IQR) of 35.3 % (106.7%). Adding a shank force ($P_{v,24} + S$ condition) again led to a significantly smaller and more typical range of changes in soleus activation relative to $P_{n,24}$ ($p = 0.0226$).

D. Center of Pressure and Kinematic Changes

Similarly, most assistance conditions did not differ from baseline (BL) in terms of the magnitude of the anteroposterior (AP) COP shift from the upright position to the squat hold, with the exception of the pelvic normal force without shank force ($P_{n,24}$) condition. A pelvic normal force increased the median magnitude of the anteroposterior (AP) COP shift from the upright position to the squat hold by 154% when compared to the shift magnitude in the baseline (BL) condition ($p < 0.0001$). The addition of a shank force ($P_{n,24} + S$) to the pelvic normal force reduced the increase in AP COP shift from BL to 42% and this condition was not significantly different from the BL condition.

The pelvic and chest trajectories of all assistance conditions differed from the BL condition. With the exception of a marginal increase in deviation from the baseline pelvic trajectory shape in the $P_{n,24}$ as compared to the $P_{n,24} + S$ condition, there were not significant differences in the pre-planned comparisons (see supplemental material).

IV. DISCUSSION

A. Assistive Force Validation

RobUST delivered vertical pelvic forces close to the desired values, with a tendency to deliver a force smaller than desired. Each load cell measuring the cable tension was separated from the end effector by two (for the shank cables) or three subsequent sheaves. Tension is lost in a velocity-dependent manner for wire rope cables routed over sheaves [20]. This

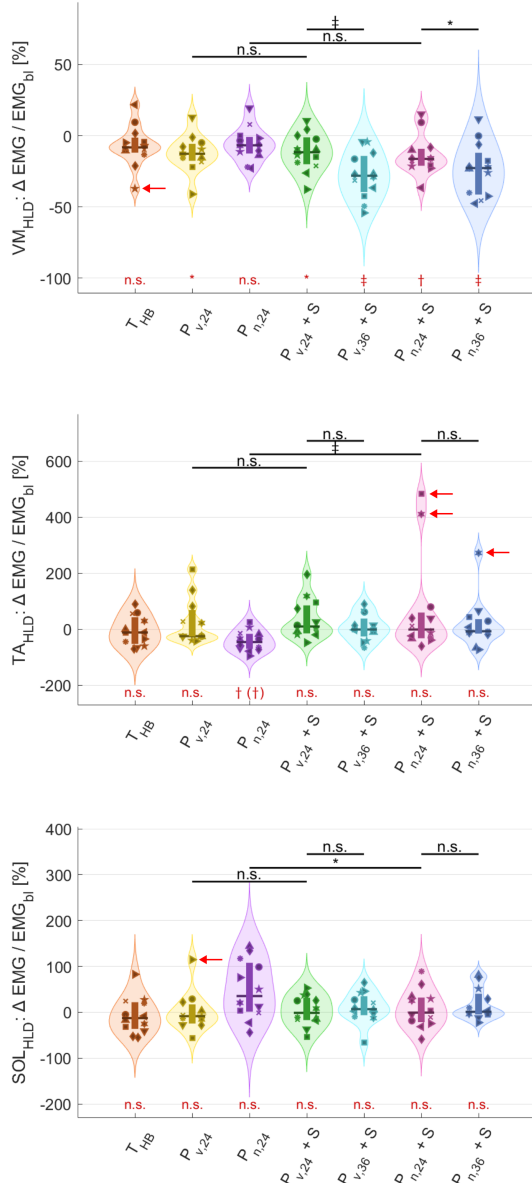


Fig. 7. Violin plots of the per-condition subject mean values for the integrated EMG during 1.5 seconds from the middle of the squat hold. The median (dark horizontal bar) and interquartile range (vertical dark bar) include outlier data and are shown along with individual subject mean data marked with unique symbols. Statistical significance for comparisons between each condition and the baseline condition are shown below each violin (n.s. → $p > 0.05$; * → $p < 0.05$; † → $p < 0.01$; ‡ → $p < 0.001$). Select pairwise comparisons are shown with connecting bars and significance presented over the bar. A small number of extreme outliers (red arrows) were present in the data but did not change the statistical significance level of any comparisons.

effect could lead to applied tensions lower or higher than desired, depending on the pelvic velocity as equilibrium is reached in the squat hold. This effect likely also impacted the application of shank forces. Misalignment between the vertical defined by the reference tracker and the normal vector to the force plate could also have contributed to achieved vertical pelvic force errors, although a post-hoc analysis showing a misalignment of only 2.3° suggests this effect was minimal. Overall, the results show the feasibility of controlling a CDRP with virtual reality trackers and approximated cable attachment

points. Increasing interest in remote robotic rehabilitation in clinical and research applications suggests that the control of rehabilitative CDRPs with affordable and portable sensors will grow in importance [21].

B. Model-Coordinated Forces Enable Targeted Assistance at the Knee

While individual subjects squatted with a relatively consistent posture across conditions, there was substantial inter-subject variability in the ankle plantar/dorsiflexion angle (θ_1) and especially in the sagittal plane pelvis-to-chest angle (θ_4). Different subject-specific squat hold kinematics led to a range of normalized knee gravity torques and, therefore, gravity torque assistance magnitudes in the squat hold. The subject who had the smallest knee gravity torque in the squat hold had a notably different posture with much larger θ_4 values (subject median $\theta_4 = 131.0^\circ$), likely due mostly to greater hip flexion. This posture moves the center of mass of the torso anteriorly and closer to the knee rotation axis, which has been shown to reduce gravity-induced knee torque [22].

Despite the variety of unique squat kinematics, for most subjects, coordinated pelvis-shank assistance reduced knee extensor (VM) activity without significantly altering ankle muscle (TA, SOL), BF, or GluMd activation. As pelvic forces increased in pelvis-shank assistance conditions, most subjects showed further VM activity reductions. Pelvis-shank assistance caused relatively small changes in COP shifts from the upright posture to the squat hold. Likewise, pelvic vertical force alone reduced VM activity without significantly altering ankle muscle activity or AP COP shift, likely because the pelvic vertical force had a relatively small moment arm about the ankle and thus generated smaller ankle torques.

In contrast, the pelvis normal force alone had a large moment arm about the ankle throughout the squat range and failed to reduce VM activity, suppressed TA activity, and led to large increases in AP COP shift from the upright position to the squat hold. All assistance conditions caused changes in the pelvic and chest trajectories of grossly similar magnitude. However, the pelvic normal force combined with a shank force caused smaller increases in the pelvic trajectory's LSED (i.e., spatial deviation) from baseline than the pelvic normal force alone (see supplemental material).

These results show that the pelvis-shank assistance conditions successfully provided targeted knee extension assistance and that the shank force was necessary to balance ankle torques generated by the pelvic normal force. A shank force to balance ankle torques was not critical for a pelvic vertical force, likely because it had a small moment-arm about the ankle.

C. Advantages of postural model-based control

A vertical pelvic force creates very little knee torque near the upright position. A pelvic normal force allowed the robot to generate substantial knee extension torques throughout the range of the squat. This feature could be particularly important for standing postural training. For example, people with severe lower limb weakness, such as those with SCI, require knee

extension assistance to stand upright [15]. A pelvic normal force paired with a posteriorly directed shank force could generate knee extension in the upright position, whereas a vertical pelvic force cannot. At the same time, the pelvic normal force generated smaller vertical force components, meaning it can provide knee extension torque while also allowing the subject to bear more of their weight. Weight-bearing is important for certain patient populations with upper motor neuron dysfunction, such as those with spinal cord injury or cerebral palsy, as it generates peripheral sensory signals that are important for sensorimotor integration and plasticity in the brain and spinal cord [23]. Additionally, the task-invariant approach of partial gravity compensation has several advantages: it does not constrain the movement towards a desired trajectory and thus encourages natural movement variability, which has been shown to be beneficial in postural motor learning; it provides an intuitive way to select the assistance level as a fraction of the gravity torques, in contrast to selecting proportional-derivative gains in impedance control; it can easily be adjusted to assist-as-needed control by increasing the gravity compensation coefficient, c in (3), at the measured edges of the postural workspace [24].

V. LIMITATIONS AND CONCLUSION

We have shown that a conceptual postural model can be used to coordinate multisegment forces in a CDPR to achieve joint-specific assistance torques. We have also shown the feasibility of controlling a CDPR with affordable sensors and approximated cable attachment points, suggesting that similar approaches could be used to control portable rehabilitative CDPRs. The coordination of multisegment forces with a biomechanical model may enable a wider range of stable postural training movements, such as maximal reaching or sit-to-stand, in more severely impaired populations. Integrating more complex in-the-loop postural models could improve the accuracy of the approach. Computer vision may represent a particularly promising approach for applying more complex models due to its low cost and ability to measure subject anthropometrics and a variety of joint angles.

- [1] V. Firouzi, A. Seyfarth, S. Song, O. von Stryk, and M. A. Sharifi, “Biomechanical models in the lower-limb exoskeletons development: a review,” *Journal of NeuroEngineering and Rehabilitation*, vol. 22, no. 1, p. 12, jan 2025.
- [2] S.-H. Hyon, J. Morimoto, T. Matsubara, T. Noda, and M. Kawato, “Xor: Hybrid drive exoskeleton robot that can balance,” in *2011 IEEE/RSJ International Conference on Intelligent Robots and Systems*, sep 2011, pp. 3975–3981.
- [3] C. Nesler, G. Thomas, N. Divekar, E. J. Rouse, and R. D. Gregg, “Enhancing voluntary motion with modular, backdrivable, powered hip and knee orthoses,” *IEEE Robotics and Automation Letters*, vol. 7, no. 3, pp. 6155–6162, jul 2022.
- [4] H. Geyer and H. Herr, “A muscle-reflex model that encodes principles of legged mechanics produces human walking dynamics and muscle activities,” *IEEE Transactions on Neural Systems and Rehabilitation Engineering*, vol. 18, no. 3, pp. 263–273, jun 2010.
- [5] A. Q. L. Keemink, T. J. H. Brug, E. H. F. V. Asseldonk, A. R. Wu, and H. V. D. Kooij, “Whole body center of mass feedback in a reflex-based neuromuscular model predicts ankle strategy during perturbed walking,” *IEEE Transactions on Neural Systems and Rehabilitation Engineering*, vol. 29, pp. 2521–2529, 2021.
- [6] G. Durandau *et al.*, “Voluntary control of wearable robotic exoskeletons by patients with paresis via neuromechanical modeling,” *Journal of NeuroEngineering and Rehabilitation*, vol. 16, no. 1, jul 2019.
- [7] P. Morasso, A. Cherif, and J. Zenzeri, “Quiet standing: The single inverted pendulum model is not so bad after all,” *PLoS One*, vol. 14, no. 3, mar 2019.
- [8] A. Alamdari and V. Krovi, “Design and analysis of a cable-driven articulated rehabilitation system for gait training,” *Journal of Mechanisms and Robotics*, vol. 8, no. 5, oct 2016.
- [9] J. Kang, D. Martelli, V. Vashista, I. Martinez-Hernandez, H. Kim, and S. K. Agrawal, “Robot-driven downward pelvic pull to improve crouch gait in children with cerebral palsy,” *Sci. Robot.*, vol. 2, no. 8, p. 2634, 2017.
- [10] E. J. Park *et al.*, “Design and preliminary evaluation of a multi-robotic system with pelvic and hip assistance for pediatric gait rehabilitation,” in *2017 International Conference on Rehabilitation Robotics (ICORR)*, jul 2017, pp. 332–339.
- [11] H. P. Aria, M. Ahrabi, F. Allahverdi, and M. H. Korayem, “Kinematic analysis and development of cable-driven rehabilitation robot for cerebral palsy patients,” *International Journal of Advanced Robotic Systems*, vol. 20, no. 1, jan 2023.
- [12] H. Faqih, M. Saad, K. Benjelloun, M. Benbrahim, and M. N. Kabbaj, “Tracking trajectory of a cable-driven robot for lower limb rehabilitation,” *International Journal of Electrical, Computer, Energy, Electronic and Communication Engineering*, vol. 10, no. 8, pp. 1015–1020, 2016.
- [13] D. Surdilovic, J. Zhang, and R. Bernhardt, “String-man: Wire-robot technology for safe, flexible and human-friendly gait rehabilitation,” in *2007 IEEE 10th International Conference on Rehabilitation Robotics*, jun 2007, pp. 446–453.
- [14] T. D. Luna, V. Santamaría, I. Omofuma, M. I. Khan, and S. K. Agrawal, “Postural control strategies in standing with handrail support and active assistance from robotic upright stand trainer (robust),” *IEEE Transactions on Neural Systems and Rehabilitation Engineering*, vol. 29, pp. 1424–1431, 2021.
- [15] E. Rejc, K. Minassian, M. Capogrosso, M. W. Keith, S. Harkema, and V. R. Edgerton, “Robotic postural training with epidural stimulation for the recovery of upright postural control in individuals with motor complete spinal cord injury: A pilot study,” *Neurotrauma Reports*, vol. 5, no. 1, pp. 277–292, mar 2024.
- [16] W. Saensook, L. Mato, N. Manimmanakorn, P. Amatachaya, T. Sooknuan, and S. Amatachaya, “Ability of sit-to-stand with hands reflects neurological and functional impairments in ambulatory individuals with spinal cord injury,” *Spinal Cord*, vol. 56, no. 3, pp. 232–238, mar 2018.
- [17] P. de Leva, “Adjustments to Zatsiorsky–Seluyanov’s segment inertia parameters,” *J. Biomech.*, vol. 29, no. 9, pp. 1223–1230, 1996.
- [18] C. Larivière, A. B. Arsenault, D. Gravel, D. Gagnon, and P. Loisel, “Evaluation of measurement strategies to increase the reliability of emg indices to assess back muscle fatigue and recovery,” *J. Electromyogr. Kinesiol.*, vol. 12, no. 2, pp. 91–102, 2002.
- [19] Y. Tao, A. Both, R. I. Silveira, K. Buchin, S. Sijben, R. S. Purves, P. Laube, D. Peng, K. Toohey, and M. Duckham, “A comparative analysis of trajectory similarity measures,” *GIScience Remote Sens.*, vol. 58, no. 5, pp. 643–669, 2021.
- [20] P. Máté and A. Szekrényes, “Measurement of the tension loss in a cable traveling over a pulley, for low-speed applications,” *Experimental Mechanics*, nov 2024.
- [21] A. Akbari, F. Haghverd, and S. Behbahani, “Robotic home-based rehabilitation systems design: From a literature review to a conceptual framework for community-based remote therapy during covid-19 pandemic,” *Frontiers in Robotics and AI*, vol. 8, jun 2021.
- [22] R. K. Straub, A. J. Barrack, J. Cannon, and C. M. Powers, “Trunk inclination during squatting is a better predictor of the knee-extensor moment than shank inclination,” *Journal of Sport Rehabilitation*, vol. 30, no. 6, pp. 899–904, aug 2021.
- [23] J. T. Eisdorfer, R. D. Smit, K. M. Keefe, M. A. Lemay, G. M. Smith, and A. J. Spence, “Epidural electrical stimulation: A review of plasticity mechanisms that are hypothesized to underlie enhanced recovery from spinal cord injury with stimulation,” *Frontiers in Molecular Neuroscience*, vol. 13, sep 2020.
- [24] J. W. Hinkel-Lipsker and M. E. Hahn, “The effects of variable practice on locomotor adaptation to a novel asymmetric gait,” *Experimental Brain Research*, vol. 235, no. 9, pp. 2829–2841, sep 2017.